NOVEM 2018
Noise and vibration emerging methods
The 6th conference, 7 – 9 May 2018
Ibiza – Spain

# AN EXTENDED TRANSFER MATRIX MODEL FOR THE SOUND INSULATION OF DUAL LEAF STRUCTURES WITH CORRUGATED PANELS AND STRUCTURAL CONNECTIONS

James F. Massaglia[1*], Andy Moorhouse[1]

[1]Acoustics Research Centre
The University of Salford, Salford M5 4WT, UK
[*]Email: j.f.massaglia@edu.salford.ac.uk

## ABSTRACT

*The transfer matrix method (TMM) was implemented both as a standalone approach and as a method of obtaining cavity infill layer effective properties in a periodic double plate model. These approaches were studied for their potential in predicting the sound insulation characteristics of corrugated dual leaf roofs, with applicability to multi-layered building elements more generally. Corrugated panels were modelled as equivalent orthotropic plates. Infill materials were modelled using both effective fluid representations and a Biot model. Available corrections were introduced to simulate diffuse laboratory conditions and enable comparisons to available laboratory sound transmission loss data. A number of diffuse TL measurements of dual leaf partitions and full roof systems were compared to the TMM. The inclusion of point-to-point connections reduces overestimation of such systems at high frequency, showing a strong influence of connector stiffness and panel damping factor on high frequency performance of systems, particularly with absorbent infill. The equivalent orthotropic plate model predicts a stronger effect of profile depth on low-mid frequency performance than in practice. The predicted TL is compared with laboratory measurements for several systems.*

## 1 INTRODUCTION

The aim of this study was the development and validation of a modelling framework for estimating the sound insulation performance (measured according to BS EN ISO 10140-2) of dual leaf roofs constructed of profiled metal cladding and layered cavity infill. The transfer matrix method (TMM) has been used extensively in modelling transmission loss and other

acoustic properties of systems with multiple layers, as well as sub-systems within a larger modelling framework.
In this work, the TMM formulation developed by Brouard [1] has been used both as a standalone model of multilayer dual leaf roof systems and as a way to obtain effective properties of cavity infill layers within these systems in the presence of structural connections, as a component of an analytical framework formulated by Smirnov [2] for point connected double plates, based on space harmonics. Existing approaches to point-to-point and line connected plates similarly model laterally infinite and geometrically periodic dual leaf systems (plate-fluid-plate) using spatial Fourier transforms to work with spatial Delta or Comb functions [3-6]. In sound insulation modelling, corrugated plates are generally handled using equivalent orthotropic plates, by having an orientation dependent bending stiffness. Work by Lam in this area has shown that sound transmission behaviour of profiled panels is influenced predominantly by vibration modes related to the profile details, however modelling of these is not straightforward, especially within dual leaf systems with structural framework.

## 2 THEORY

The following is a brief summary of the modelling approaches under study; more detail on each component is available in [7].

### 2.1 Definitions and the Transfer Matrix Method

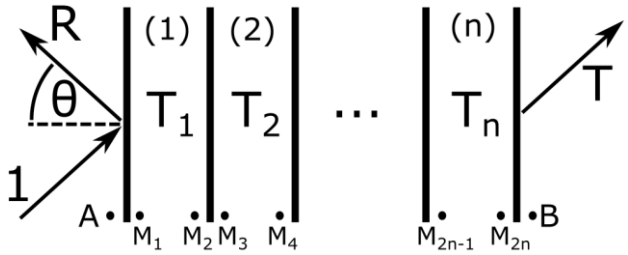

Figure 1: Transfer Matrix Method diagram (notation from [1])

The TMM formulation developed by Brouard [1] is used in this work. This approach allows modelling laterally infinite systems of layered fluids, linear elastic solids, Kirchhoff thin plates and poroelastic materials. The layers are placed between two fluid half-spaces (air) to model the transmission of airborne sound through a multilayer partition. The outputs of the TMM used in this work are the reflected and transmitted pressure wave amplitudes, R and T, for an incident plane wave $p_i$ of amplitude $I = 1$:

$$p_i(x, y, z) = Ie^{i(\mathrm{k_x}x+\mathrm{k_y}y+k_z z)} \tag{1}$$

Harmonic time dependence $e^{i\omega t}$ is assumed. Here the wavenumber components $k_x$, $k_y$ and $k_z$ satisfy the Helmholtz equation, and are defined in spherical coordinates in terms of the wavenumber in air $k_0$, angle of incidence $\theta$ and polarisation $\phi$:

$$\begin{aligned} k_x &= k_0 \sin\theta \cos\phi \\ k_y &= k_0 \sin\theta \sin\phi \\ k_z &= k_0 \cos\theta \end{aligned} \tag{2}$$

## 2.2 Porous material characterisation

Low density porous materials were modelled using the well-known Delany-Bazley formulae based on flow resistivity and porosity of the materials [8]. For high density materials (>30kg/m³), a Biot model was used, where most material properties were determined using assumptions valid for fibrous materials, found in Allard and Atalla [9].
The remaining properties of mineral wool samples – Young's modulus, flow resistivity and loss factor – were obtained by fitting modelled surface impedance for a rigidly backed material to impedance tube measured values of the required mineral and glass wool samples (using the two microphone method). For high density materials, the Young's modulus determined the location of a low frequency quarter wavelength frame resonance which was clearly identifiable. For lower density materials, the Delany-Bazley formulae were sufficient, with only flow resistivity being determined.

## 2.3 Structural connection framework

### *2.3.1 System description*

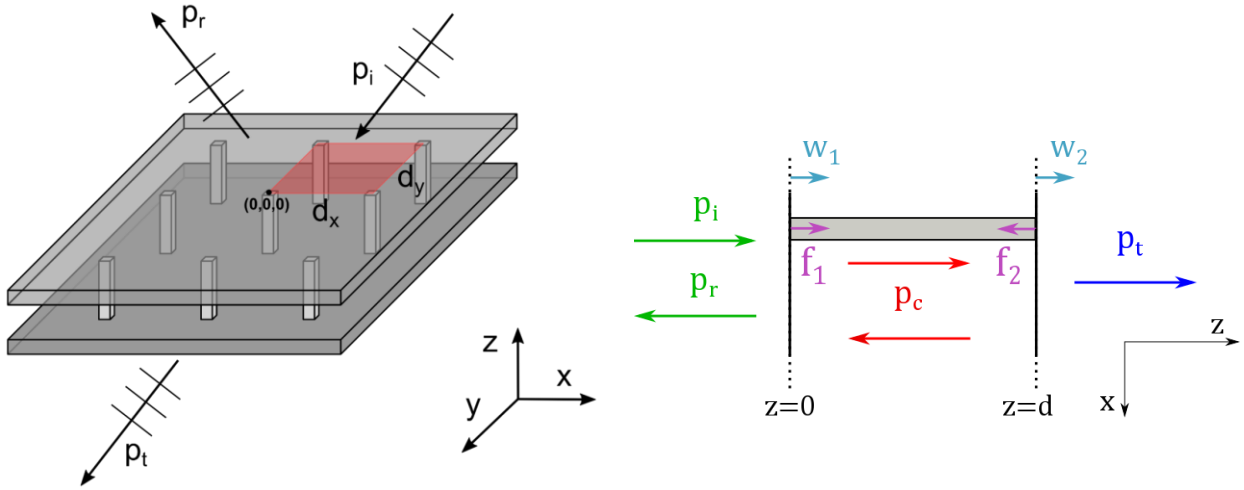


Figure 2: Double plate system with periodically spaced connecting rods and unit cell area $d_x d_y$

A model of periodically point connected laterally infinite plates separated by a fluid cavity, based on work by Smirnov [2] was used to account for structural connections. Figure 1 shows diagrams of the system. All pressure and velocity fields obey the Floquet condition, in order to account for the periodicity of the incident wave and of the geometry; a field $p$ takes the following form at intervals of $d_x$ and $d_y$:

$$p(x + d_x, y + d_y) = p(x, y)e^{i(\mathrm{k_x}d_x + \mathrm{k_y}d_y)} \tag{3}$$

The cavity between the two plates is a single fluid layer with wavenumber $k_c$ and density $\rho_c$. In this work, these values are obtained from the TMM output for layered infill, as detailed later.
Space harmonic representations were employed; the periodic component of each field (in $d_x$ and $d_y$) is expressed as a Fourier series - a plane pressure wave $p$ in a fluid space is

represented as a summation over exponentials $e^{i(\mathrm{k_x}x+\mathrm{k_y}y)}e^{i(\frac{2\pi m}{d_x}x+\frac{2\pi n}{d_y}y)} = \psi_{mn}$, where $m$ and $n$ are integers, each with a coefficient $A_{mn}$:

$$p(x,y,z) = \sum_{m,n} A_{mn}\,\psi_{mn} e^{ik_{z_{mn}}z} \tag{4}$$

Here $k_{z_{mn}}^{\,2} = k^2 - \left(k_x + \frac{2\pi m}{d_x}\right)^2 - \left(k_y + \frac{2\pi n}{d_y}\right)^2$, where $k$ is the wavenumber in the medium; this formulation satisfies the Helmholtz equation in a fluid domain. This representation allows solving system equations mode-by-mode by exploiting the orthogonality of each mode, provided that all fields are expressed in this form.
The incident wave is written in terms of Fourier coefficients $I_{mn}$, which are set to zero for all modes except where $m = n = 0$, where $I_{00} = 1$:

$$p_i = \sum_{m,n} I_{mn}\,\psi_{mn} e^{-ik_{z_{mn}}z} \tag{5}$$

Reflected and transmitted pressure fields, $p_r$ and $p_t$, are given in terms of coefficients $R_{mn}$ and $T_{mn}$, which are the scattered pressure wave amplitudes (for each harmonic) above and below the plates, from which reflection and transmission coefficients are obtained.
Velocities and displacements are obtained from these pressures using Euler's equation.
The two outer plates were modelled on the Kirchoff thin plate approximation, using the usual fourth order differential equation in terms of normal velocity. For the top plate, with bending stiffness $B_1$ and mass per unit area $m_1'$, at z=0:

$$(B_1\nabla^4 - \omega^2 m_1')\mathrm{w}_1 = p_i + p_r - p_c - f_1 \tag{6}$$

where $p_c$ is the pressure field in the cavity fluid and $f_1$ the reaction force from all connectors on the top plate, $w_1$ the plate normal displacement. For the bottom plate, with bending stiffness $B_2$ and mass per unit area $m_2'$, at z=d:

$$(B_2\nabla^4 - \omega^2 m_2')\mathrm{w}_2 = p_c - p_t - f_2 \tag{7}$$

where $p_t$ is the pressure below the bottom plate (transmitted into the receiving space), $w_2$ the normal displacement and $f_2$ the reaction force from the connectors. The terms $f_1$ and $f_2$ can represent different types of elements (line or point connections, added masses, etc.), and are written as a generic space harmonic series:

$$f_{1,2} = \sum_{m,n} F_{1,2_{mn}}\,\psi_{mn} \tag{8}$$

Continuity of normal velocity along the plates was enforced, so that sufficient conditions were set to solve the system equations, giving values for $R_{mn}$ and $T_{mn}$, the coefficients for the reflected and transmitted pressure harmonic series, in terms of the coefficients for the reaction forces $F_{1_{mn}}$ and $F_{2_{mn}}$ and the incident wave amplitude $I_{mn}$.

*2.3.2 Point-to-point connections*

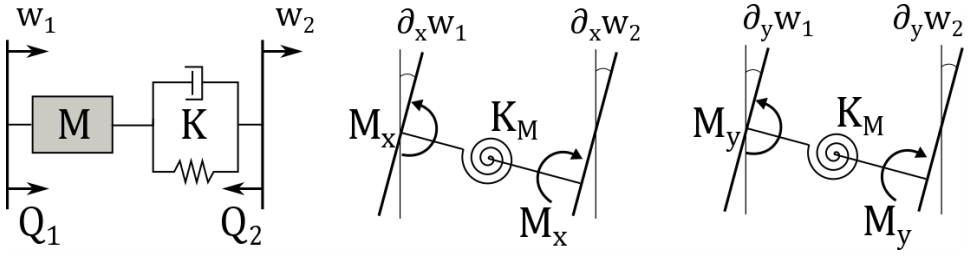


Figure 3: Point-to-point connection forces Q, moments M and displacements w (notation from [4])

Point forces ($Q_1$ and $Q_2$) and moments ($M_x$ and $M_y$) for the connector at x=0 and y=0 are sufficient to characterise the total reaction field from the connectors, $f_1$ (top plate) and $f_2$ (bottom plate):

$$f_{1,2} = \sum_{m,n} \frac{\mathrm{Q}_{1,2} + ik_{x_m} M_x + ik_{y_n} M_y}{d_x d_y} \psi_{mn} \tag{9}$$

Connecting elements were modelled as infinitesimally thin rods, so that these were transparent to waves in the cavity fluid. The forces and moments of the first connector at x=0 and y=0 are related to the point displacements $w_1$ and $w_2$ either side of the connector by a compressional stiffness matrix $K_{ij}$, and moment stiffness $K_M$:

$$\begin{bmatrix} Q_1 \\ Q_2 \end{bmatrix} = \begin{bmatrix} K_{11} & K_{12} \\ K_{21} & K_{22} \end{bmatrix} \begin{bmatrix} -w_1(0,0) \\ w_2(0,0) \end{bmatrix} \tag{10}$$

$$M_x = K_M\big(\partial_x w_1(0,0) - \partial_x w_2(0,0)\big) \tag{11}$$

$$M_y = K_M\left(\partial_y w_1(0,0) - \partial_y w_2(0,0)\right) \tag{12}$$

Displacements are then derived from the pressure series expressions to solve for the forces and moments. Full details are available in [7] for connectors with finite compressional stiffness. Model outputs in the Results section neglect connector moments; the compressional stiffness matrix elements used in plotted data were derived from a simple thin elastic rod model supporting longitudinal waves.

## 2.4 Combination with TMM

The cavity effective fluid properties are obtained from the reflection and transmission coefficients R and T calculated with the TMM for an arbitrary configuration of layers, with the method outlined in Fokin et al [10].

The wavenumber and impedance of the cavity fluid of thickness d (made of a single material or several layered materials) for a given input wavenumber $k_0$ and impedance $z_0$ are given by:

$$k_{z_c}(\theta, \phi) = \frac{-i\log x + 2\pi q}{d}, q \in Z \tag{13}$$

$$z_c(\theta,\phi) = \frac{z_0 r}{(1 - 2R + R^2 - T^2)} \tag{14}$$

where $r = \pm\sqrt{(R^2 - T^2 - 1)^2 - 4T^2}$ and $x = \frac{1-R^2+T^2+r}{2T}$. These properties should be calculated for each space harmonic m, n; however, for common mineral wool and glass wool materials, using only the zeroth harmonics is often sufficient and reduces calculation times. When including solid materials in the cavity, it becomes necessary to include higher order modes as there will be a sharper variation in effective wavenumber for different incident excitation wavenumbers. In most cases where solid boards (such as CPB or plasterboard) are present in roof systems they are mounted in direct contact with the outer metal sheets. The chosen approach in these instances was to obtain the effective combined bending stiffness of the panels as if they were fully bonded, so that the effective fluid properties of only the mineral or glass wool layers in between were obtained; comparisons with measurement are available in [7].

This approach, by including only longitudinal pressure waves, neglects the coupling of solid waves between the infill and the outer plates in a dual leaf system, which can be a limit when modelling structures with bonded cavity materials as will be seen later in the Results section.

### 2.5 Corrugated plates

Corrugated plates are modelled as equivalent orthotropic plates, based on formulae for the area moment of inertia of the geometry of trapezoidal plates, found in Bies and Hansen [11], giving distinct values of bending stiffness in each dimension: $B_x$, $B_y$ and $B_{xy}$. Within the equation of motion of each plate:

$$\left(B_x {k_x}_m^{\,4} + B_y {k_y}_n^{\,4} + B_{xy} {k_x}_m^{\,2} {k_y}_n^{\,2} - \omega^2 m'\right) w = f \tag{15}$$

### 2.6 Diffuse Transmission Loss

For the pure TMM, transmission loss is obtained from the transmission coefficient T for each angle of incidence:

$$\tau(\theta,\phi) = |T|^2 \tag{16}$$

For the point-connected plate output, the transmission coefficient results from a summation of all travelling modes:

$$\tau(\theta,\phi) = \sum_{m,n} \frac{Ap_t v_t}{Ap_i v_i} = \sum_{m,n} \frac{\mathrm{k_{z}}_{mn} |T_{mn}^2|}{\mathrm{k_{z}}_{00} |I_{00}^2|} \tag{17}$$

Modes where $k_{z_{mn}} > k_0$ are simply discarded, as these represent evanescent waves that do not travel into the far field.

The diffuse transmission loss for laterally infinite systems differs from measured values for finite structures. Two corrections to the calculated transmission coefficient were employed simultaneously; one to reduce the amount of incident energy towards grazing angles, by applying a Gaussian weighting $G$ as found in Kang et al. [12]: $G(\theta) = e^{-\beta\theta^2}$, where $\beta$ is a factor dependent on the room characteristics (a value of $\beta = 1$ is used in Results presented here). This approach is somewhat more justifiable than 'field incidence', a hard limit to the incidence angle $\theta$ (typically around 78 degrees).

A correction for finite structure size makes use of the radiation efficiency $\sigma_R$ of a finite rectangular structure, derived from the Rayleigh integral, and referred to as spatial windowing [13]. The formulation outlined by Rhazi and Atalla [14] was used, and applied to the transmission coefficient. Obtaining the radiation efficiency requires numerical integration, and with this approach it can be cheaply calculated using fixed-point quadrature. As the maximum trace wavenumber is increased, however, integral convergence is slower and particular care should be taken – here adaptive techniques are to be preferred over fixed point evaluations. This is especially the case when integrating over wavenumbers greater than the maximum wavenumber in air (required e.g. when obtaining radiated sound power for a point force).
The expression for the transmission coefficient, with corrections for finite size and laboratory diffusivity, is:

$$\tau_F = \tau(\theta, \phi)\sigma_R(\theta, \phi)G(\theta) \tag{18}$$

At each frequency, the diffuse transmission coefficient results from integration over angles $\theta$ and $\phi$:

$$\tau_{diff} = \frac{\int_0^{2\pi} \int_0^{\frac{\pi}{2}} \tau_F(\theta, \phi) \sin\theta \cos\theta \, d\theta d\phi}{\int_0^{2\pi} \int_0^{\frac{\pi}{2}} \sin\theta \cos\theta \, d\theta d\phi} \tag{19}$$

Diffuse transmission loss (TL) is given by:

$$TL = -10 \log \tau_{diff} \tag{20}$$

A naïve Monte-Carlo approach was used to integrate the transmission coefficient in 120 logarithmically spaced frequency bins between 40 and 6000Hz, by picking pseudorandom pairs (from Halton sequences) of angles θ and ϕ over a hemisphere. This approach avoids the common pitfalls of fixed point evaluations for this kind of problem, where particular combinations of angles that produce large peaks in response can often be missed (especially at and above panel critical frequencies). Convergence was defined as the error estimate reached 0.01dB.
Results compared with laboratory measurements are averaged in 1/3 octave bands.

## 3 RESULTS

### 3.1 FEM comparisons

Figure 3 shows the analytical and FEM models of transmission loss through a laterally infinite double plate system (plate-air-plate) with 5mm thick aluminium plates (rho = 2700, E = 70e9) connected by rods (100mm by 100mm spacing) with varying Young's modulus, for incidence angle $\theta = \frac{\pi}{4}$. The analytical model is the framework from Section 2.3 with point-to-point connectors modelled as thin elastic rods supporting longitudinal waves. These results include near field effects, and use Floquet boundary conditions in COMSOL for an infinite.

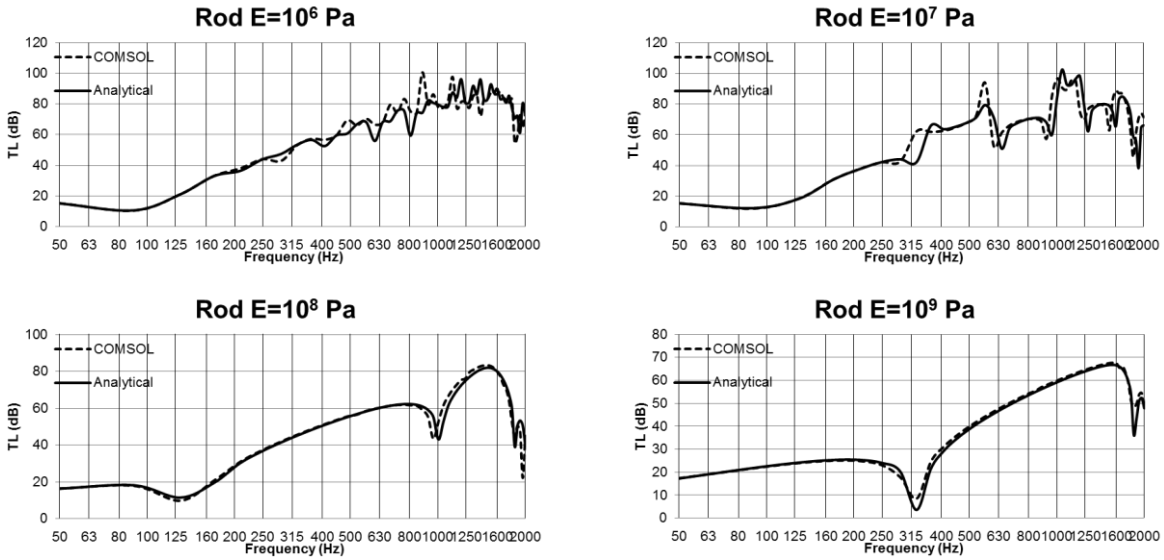


Figure 3: Comparison of analytical and FEM calculated transmission loss through a laterally infinite periodic aluminium double plate structure with point connections at 100mm by 100mm spacing for an incident plane wave at $\theta = \frac{\pi}{4}$, with rod Young's modulus varying from $10^6$ to $10^9$

Good agreement is found throughout the frequency range. The plots show that increases in connector compressional stiffness cause an increase in low frequency mass-spring-mass resonance, as the total cavity stiffness is increased. A decrease in stiffness increases TL above the mass-spring-mass resonance, though additional dips are introduced as the wavelength approaches the rod length.

### 3.2 Rooflight (no cavity absorption)

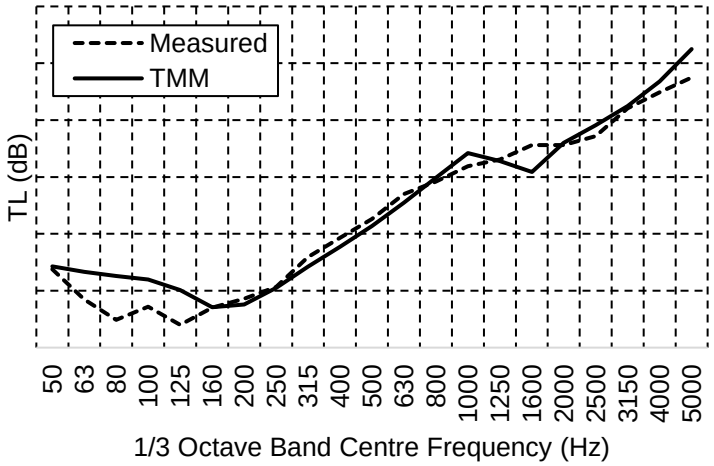


Figure 4: Measured diffuse transmission loss of rooflight with two corrugated GRP sheets of 1.3mm thickness compared to TMM model; y axis gridlines at 10dB intervals

Figure 4 shows the laboratory measured 1/3 octave band transmission loss of a rooflight with 1.3mm corrugated glass-reinforced polycarbonate sheets separated by an air cavity, plotted with modelled TMM modelled values. Despite the overestimation of mass-air-mass resonant frequency (160-200Hz vs 80-100Hz), there is good agreement overall using only the TMM.

Introducing connectors has a small effect on transmission loss, as the small amount of absorption in the cavity makes the airborne path dominate the response.

### 3.3 Simple corrugated roofs with mineral wool infill

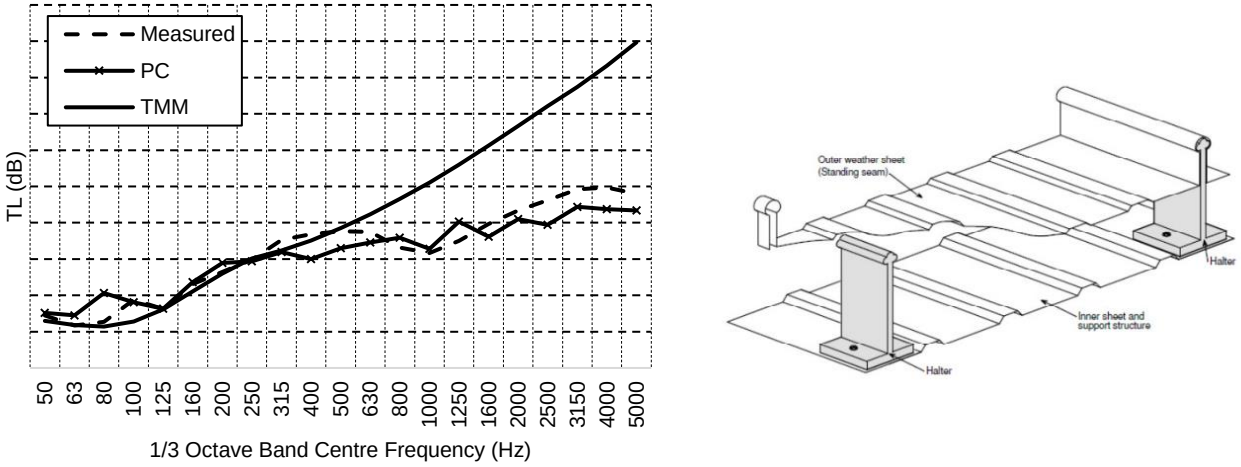


Figure 5: Diffuse field transmission loss of standing seam corrugated roof system with soft fibrous infill and halters; vertical axis gridlines at 10dB intervals; measured (solid line) versus periodic point-connected model (dashed) and TMM (dotted)

Figure 5 shows the diffuse transmission loss in 1/3 octave bands of a standing seam roof system with a 0.9mm corrugated aluminium top sheet and a 0.7mm corrugated bottom sheet (liner) and a single layer of mineral wool infill. Connecting the outer plates are aluminium halters at 400mm spacing, as shown in the diagram above. The TMM model (with necessary corrections for size and diffusivity) overestimates performance above 500Hz. The complete model with point connections, modelled as simple rods supporting longitudinal waves, is much closer to measured values throughout the range, and includes an observed shifted mass-spring-mass resonance at 125Hz due to connector stiffness. The path through the structural connections dominates the response at high frequency, where the absorptive material minimises airborne transmission through the cavity. Nonetheless, both modelling frameworks achieve good agreement from 50 to 500Hz in this case.

The same cannot be said of system shown in Figure 6. In this case, both inner and outer metal sheets are identical, 0.9mm thick corrugated steel with the same profile geometry, and a layer of low density mineral wool. The orthotropic plate formulation employed in the models shows a peak at 250Hz and subsequent dip at 500Hz, as a result of the lower critical frequency (associated with the stiffest dimension along the profile ribs) being in the same location for both plates, leading to poor results above 100Hz. Comparisons of measured TL of single corrugated metal panels have shown no strong low critical frequency dip and a response at low frequency which appears only weakly dependent on profile depth, suggesting orthotropic behaviour is not exhibited in the frequency range of interest [7].
The point-connected plate model underestimates TL at high frequency. While FEM modelled connector stiffness was used, the more complex nature of the framework requires modelling beyond the individual connection, to include the junctions between the connectors and supporting beams, with staggered fixings, which potentially reduce stiffness as seen by the plates to a degree.

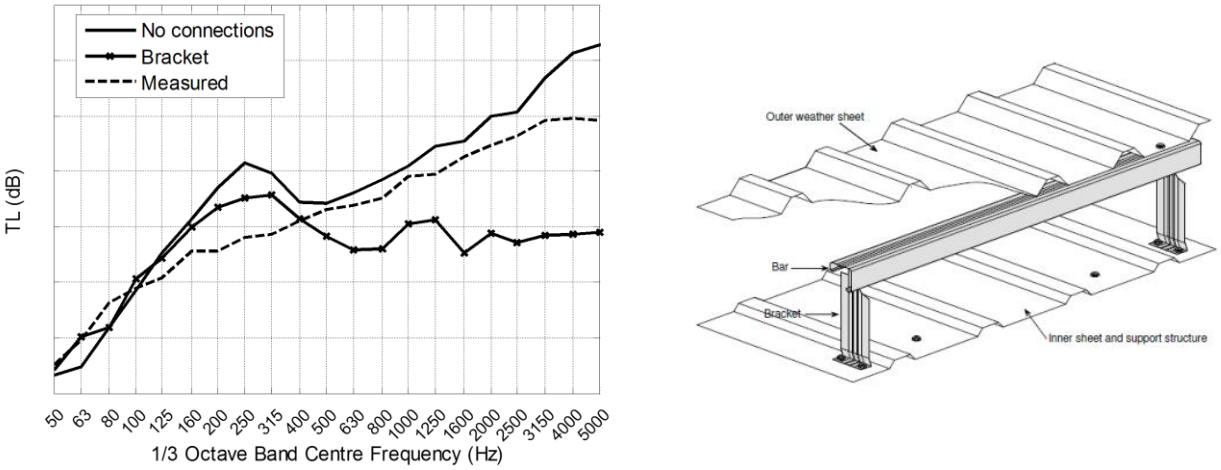


Figure 6: Diffuse transmission loss of corrugated metal roof with bracket connectors against TMM model ('No connections') and point-connected plate model with FEM-derived bracket connector stiffness ('bracket'); y axis in 10dB steps

TL at high frequency is also influenced, within the model, by the panel loss factor. This controls the slope above the critical frequency. Increasing panel loss factor was found to improve fit over a range of common cladding; the use of experimental damping coefficients may improve model performance while maintaining the computationally cheap equivalent orthotropic plate formulation for cladding, however all the caveats regarding its limitations should be kept in mind. Robust improvement of these models is predicated on a detailed characterisation of the corrugated panel response, one that accounts for profile geometry and which would display modal behaviour more in line with observations.

### 3.4 Roof with layered high density infill

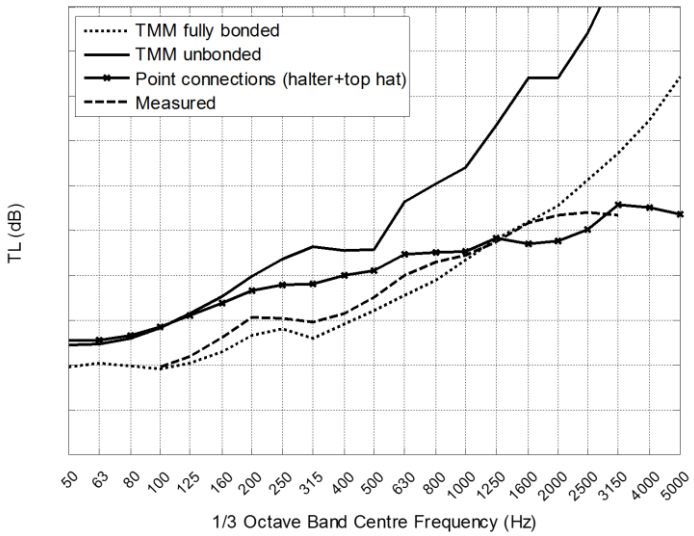


Figure 7: Comparison of measured and modelled diffuse TL of roof structure with four layers of high density mineral wool (>200kg/m$^3$) – model configurations are pure TMM ('fully bonded'), pure TMM with small air layers separating the infill from the outer metal panels ('unbonded') and the model with periodic point connections; y axis gridlines in 10dB steps

Figure 7 shows the measured and modelled diffuse TL of a standing seam roof with corrugated aluminium and steel outer sheets, four layers of high density mineral wool in the cavity (200kg/m3), and halter connectors.
The approaches chosen to model this system were:

1. 'TMM fully bonded': a pure TMM with poroelastic infill layers in contact with the outer metal sheets.
2. 'TMM unbonded': a pure TMM model with small (0.01mm) air gaps mechanically separating the infill from the outer metal sheets.
3. 'Point connections': infill layers modelled as effective fluid layer in point-connected plate model, with FEM derived stiffness of connectors – this approach produces no mechanical coupling between infill layers and outer metal sheets.

The TMM model with fully bonded layers is closest to measurement results, and shows the influence of mechanical coupling of infill with the metal sheets; overall the TL is lower and a dip at 315Hz can be seen, associated with the mechanical stiffness of the infill. In order to account for this within the point connection framework, it is necessary to model the cavity layer as a solid or poroelastic medium, and to also include the effect of shear stress at the boundary between the cavity and the outer plates. For this reason, approaches 2 and 3, neglecting mechanical coupling of the infill, on the whole overestimate TL, even though approach 3 shows the usual decrease in TL at high frequency associated with the structure-borne path through the connectors.

## 4 CONCLUDING REMARKS

Pure transfer matrix models show good agreement for structures with no cavity infill, and for structures where there is a significant structure-borne path through the infill (high density materials in contact with outer panels). In other cases where there is light or uncompressed cavity infill, common roof constructions, the TMM alone overestimates TL at high frequency, with discrepancies that can exceed 20-30dB. However, the TMM in combination with a model for point connections produces good predictions across the frequency range for standing seam constructions. For constructions employing more complex brackets, the agreement is less good. The following aspects of the model are likely to bring about improved prediction in this case:

1. **Orthotropic plate model**: TL throughout the frequency range, and especially at high frequency, is not well characterised by the equivalent orthotropic plate model for corrugated panels. More detailed models of the profile geometry would address this issue.
2. **Corrugated panel damping**: Changes in damping factor within the models control the high frequency response of modelled single and dual leaf systems; using experimental frequency-dependent damping data for corrugated plates may improve performance without resorting to a more complex model
3. **Stiffness of connectors**: for point-to-point connectors, compressional stiffness has a large impact on overall transmission loss, and especially at high frequency in the presence of absorbent infill; when using FEM modelled stiffness, TL was still generally underestimated meaning measured data may be an avenue for improvement

## 5 ACKNOWLEDGEMENTS

Many thanks to the MCRMA and the University of Salford Acoustic Laboratories for funding the project, to Andy Elliott for carrying out an extensive literature survey and setting a clear direction for the research, and to Dmitry Smirnov for crucial theoretical work and guidance.

## REFERENCES


[1] B. Brouard, D. Lafarge, and J. Allard, “A general method of modelling sound propagation in layered media,” *J. Sound Vib.*, vol. 183, pp. 129–142, 1995.

[2] D. Smirnov, “Sound transmission through two elastic plates interconnected by rods,” *Intern. Doc.*, 2015.

[3] G.-F. Lin, “Sound transmission through periodically framed parallel plates,” *J. Acoust. Soc. Am.*, vol. 61, p. 1014, 1977.

[4] D. Takahashi, “Sound radiation from periodically connected double-plate structures,” *J. Sound Vib.*, vol. 90, no. 4, pp. 541–557, 1983.

[5] J. Brunskog, “The influence of finite cavities on the sound insulation of double-plate structures,” *J. Acoust. Soc. Am.*, vol. 117, no. 6, p. 3727, 2005.

[6] F. X. Xin and T. J. Lu, “Transmission loss of orthogonally rib-stiffened double-panel structures with cavity absorption.,” *J. Acoust. Soc. Am.*, vol. 129, no. 4, pp. 1919–34, May 2011.

[7] J. F. Massaglia, “Modelling the sound insulation of corrugated roof structures: an extended transfer matrix approach,” The University of Salford, 2017.

[8] M. E. Delany and E. N. Bazley, “Acoustical properties of fibrous absorbent materials,” *Appl. Acoust.*, vol. 3, no. 2, pp. 105–116, 1970.

[9] J. Allard and N. Atalla, *Propagation of Sound in Porous Media*. John Wiley and Sons, 2009.

[10] V. Fokin, M. Ambati, C. Sun, and X. Zhang, “Method for retrieving effective properties of locally resonant acoustic metamaterials,” *Phys. Rev. B - Condens. Matter Mater. Phys.*, vol. 76, no. 14, p. 144302, Oct. 2007.

[11] D. A. Bies and C. H. Hansen, *Engineering noise control : theory and practice*, vol. 3. 2003.

[12] H. Kang, J. Ih, J. Kim, and H. Kim, “Prediction of sound transmission loss through multilayered panels by using Gaussian distribution of directional incident energy,” *J. Acoust. Soc. Am.*, vol. 107, no. 3, pp. 1413–20, Mar. 2000.

[13] M. Villot, C. Guigou, and L. Gagliardini, “Predicting the Acoustical Radiation of Finite Size Multi-Layered Structures By Applying Spatial Windowing on Infinite Structures,” *J. Sound Vib.*, vol. 245, no. 3, pp. 433–455, Aug. 2001.

[14] D. Rhazi and N. Atalla, “A simple method to account for size effects in the transfer matrix method,” *J. Acoust. Soc. Am.*, vol. 127, no. 2, p. EL30-EL36, 2010.